Novel Re(I) dendrimers: synthesis, characterization and theoretical studies†

Zhenjun Si,[a,b] Xiaona Li,[a] Xiyan Li,[a] Guohai Xu,[a] Chenling Pan,[a] Zhiyong Guo,[a] Hongjie Zhang*[a] and Liang Zhou[a]

Received 30th June 2009, Accepted 28th September 2009
First published as an Advance Article on the web 30th October 2009
DOI: 10.1039/b912939a

Four novel diimine rhenium(I) carbonyl complexes with the formula [Re(CO)$_3$(**L**)Br], where **L** = 2-(4-(9*H*-carbazol-9-yl)phenyl)-1*H*-imidazo[4,5-f][1,10]phenanthroline (**P1**), 2-(4-(3,6-di-*tert*-butyl-9*H*-carbazol-9-yl)phenyl)-1*H*-imidazo-[4,5-f][1,10]phenanthroline (**P2**), 2-(4-(6-(9*H*-carbazol-9-yl)-9*H*-3,9′-bicarbazol-9-yl)phenyl)-1*H*-imidazo[4,5-f][1,10]phenanthroline (**D1**), and 2-(4-(3′,6′-di-*tert*-butyl-6-(3,6-di-*tert*-butyl-9*H*-carbazol-9-yl)-9*H*-3,9′-bicarbazol-9-yl)phenyl)-1*H*-imidazo[4,5-f][1,10]phenanthroline (**D2**), have been successfully synthesized and fully characterized by ^{1}H NMR, IR, and UV–Vis, *etc.* The luminescence quantum yields (LQYs) of the parent Re(I) complexes **P1** and **P2** are 0.13 and 0.16, respectively, which are much higher than the previously reported Re(I) dendrimers. The HOMOs and the LUMOs of **P1** and **P2** are calculated to be mainly composed of [d(Re) + π(CO + Br)] and π*(**L**) orbital, respectively. However, those of the Re(I) dendrimers **D1** (LQY = 0.066) and **D2** (LQY = 0.0048) are mainly localized on ligand **L**, indicating that the component of the metal-to-ligand charge-transfer dπ (Re) → π*(N–N) (MLCT) transitions in **P1** and **P2** should be more than those in **D1** and **D2**. As a result, the higher LQYs of **P1** and **P2** are tentatively assigned to the disturbance of the MLCT transitions during the photoluminescence process.

Introduction

The study of the control of the photochemical, photophysical, and electrochemical properties of transition metal complexes is a hot topic due to the advantages of their diverse applications,[1–8] which has led to intensive studies of d^6 transition metal diimine complexes including Ru(II), Ir(III), Pt(II), and Re(I). One of the most efficient methods of tuning the properties of these complexes is to change the properties and/or scale of the organic ligand. For example, it is reported that purposefully designed dendrimers can offer excellent luminescence properties,[9–11] and it was recently found that the luminescence quantum yield (LQY) of the Re(I) dendrimer based on phenanthroline derivatives could be much higher than that of the corresponding parent Re(I) complex due to the suppression of the T–T annihilation by encapsulating the emitting centers.[12]

According to the fact that the complexation of phenanthroline derivatives with ions of transition metals and lanthanides provides a virtually countless library of coordination compounds and their rigidity gives them entropically better chelating abilities,[13] we report, in this paper, the synthesis of several novel phenanthroline derivatives and the corresponding Re(I) complexes **P1**, **P2**, **D1** and **D2** as well as experimental and theoretical studies on their photophysical properties. The LQYs of **P1** and **P2** in CH$_2$Cl$_2$ are 0.13 and 0.16, respectively, which are much higher than that (0.03) of a previously reported Re(I) dendrimer.[12] The higher LQYs of **P1** and **P2** could be partly attributed to the larger contributions of the metal-to-ligand charge-transfer dπ(Re) → π*(L) (MLCT) transitions of **P1** and **P2** according to the theoretical calculations.

Experimental section

Materials

N,N-Dimethylacetamide (DMA) was dried with P$_2$O$_5$, the carbazole (**R1**) and other chemicals are commercially available and used without further purification. 3,6-Diiodo-9-tosyl-9*H*-carbazole (I$_2$TsCz), 3,6-di-*tert*-butyl-9*H*-carbazole (**R2**), 6-(9*H*-carbazol-9-yl)-9*H*-3,9′-bicarbazole (**R3**), 3,6-di-*tert*-butyl-9-(3-(3,6-di-*tert*-butyl-9*H*-carbazol-9-yl)-9*H*-carba-zol-6-yl)-9*H*-carbazole (**R4**), 4-(9*H*-carbazol-9-yl)benzaldehyde (**a**), 4-(3,6-di-*tert*-butyl-9*H*-carbazol-9-yl)benzaldehyde (**b**), 4-(6-(9*H*-carbazol-9-yl)-9*H*-3,9′-bicarbazol-9-yl)benzaldehyde (**c**), and 4-[3,6-bis(3,6-di-*tert*-butyl-9*H*-carbazol-9-yl)-9*H*-carbazol-9-yl]benzaldehyde (**d**) were prepared according to the literature.[14]

Synthesis of L1

1,10-Phenanthroline-5,6-dione (0.420 g, 2.000 mmol), compound **a** (0.540 g 2.000 mmol), and NH$_4$OAc (1.540 g, 20.000 mmol) were added to 15 mL HOAc. The mixture was refluxed for 6 h. The crude product was poured into 100 mL H$_2$O and stirred for 15 min. The resulting yellow powder was collected by filtration and

---

[a] *State Key Laboratory of Rare Earth Resource Utilization, Changchun Institute of Applied Chemistry, Chinese Academy of Sciences, Changchun, 130022, People's Republic of China. E-mail: hongjie@ciac.jl.cn; Fax: +86 43185698041; Tel: +86 431 85262127*

[b] *School of Materials Science and Engineering, Changchun University of Science and Technology, Changchun, 130022, People's Republic of China. E-mail: sizj168@126.com; Fax: +86 43185583015; Tel: +86 43185583016*

† Electronic supplementary information (ESI) available: Tables S1–S4, Fig. S1–S5: selected bond lengths and angles, frontier molecular orbital compositions, triplet absorption parameters, absorption spectra of L1–L4 and electron density plots. CCDC reference numbers 722314 and 722315. For ESI and crystallographic data in CIF or other electronic format see DOI: 10.1039/b912939a

washed successively with 10 mL dilute aqueous NaOH solution, 50 mL H_2O, and 10 mL methanol to get 0.740 g (80%) of yellow powder. ^{1}H NMR ($CDCl_3$, 400 MHz): δ 7.26 (5H, s), 7.29 (2H, d, $J = 8.8$), 7.41 (2H, d, $J = 8.8$), 7.52 (1H, m), 7.94 (1H, m), 8.09 (2H, s), 8.81–8.96 (3H, m), 9.21–9.22 (1H, s), 14.40 (1H, s). Anal. Calcd for $C_{31}H_{19}N_5$: C, 80.68; H, 4.15; N, 15.17. Found: C, 80.35; H, 4.39; N, 15.26%. IR (KBr): v 1452, 1607, 3465 cm^{-1}.

Synthesis of L2

The procedure is similar to that of **L1**. Yield: 75%. ^{1}H NMR ($CDCl_3$, 400 MHz): δ 1.48 (18H, s) 7.44 (5H, d, $J = 8.8$), 7.49 (1H, d, $J = 3.2$), 7.52 (2H, d, $J = 3.2$), 7.70 (1H, s), 7.77 (3H, d, $J = 8.4$), 8.16 (2H, s), 8.50 (2H, d, J = 6.4), 9.12–9.18 (3H, m), 10.64 (1H, s). Anal. Calcd for $C_{39}H_{35}N_5$: C, 81.64; H, 6.15; N, 12.21. Found: C, 81.45; H, 6.45; N, 12.10%. IR (KBr): v 1449, 1608, 3426 cm^{-1}.

Synthesis of L3

The procedure is similar to that of **L1**. Yield: 84%. ^{1}H NMR ($CDCl_3$, 400 MHz): δ 7.29–7.31 (7H, m), 7.38–7.43 (10H, m), 7.60–7.69 (4H, m), 7.75 (1H, d, $J = 8.4$), 7.83 (1H, d, $J = 8$), 7.98 (1H, d, $J = 8$), 8.15–8.17 (5H, m), 8.25–8.30 (3H, m), 8.57 (1H, d, $J = 8$), 10.20 (1H, s). Anal. Calcd for $C_{55}H_{33}N_7$: C, 83.42; H, 4.20; N, 12.38. Found: C, 83.75; H, 4.02; N, 12.23%. IR (KBr): v 1451, 1599, 3406 cm^{-1}.

Synthesis of L4

The procedure is similar to that of **L1**. Yield: 70%. ^{1}H NMR ($CDCl_3$, 400 MHz): δ 1.46 (36H, s), 7.32–7.35 (5H, m), 7.45–7.47 (5H, m), 7.63–7.65 (3H, m), 7.79 (3H, m), 7.90 (1H, m), 7.96–7.98 (1H, d, $J = 8.4$), 8.03–8.08 (1H, m), 8.16 (4H, s), 8.24–8.26 (3H, m), 8.54 (1H, d, $J = 8$), 9.18 (1H, d, $J = 10$), 10.19 (1H, s). Anal. Calcd for $C_{71}H_{65}N_7$: C, 83.91; H, 6.45; N, 9.65. Found: C, 84.17; H, 6.57; N, 9.26%. IR (KBr): v 1490, 1602, 3406 cm^{-1}.

Synthesis of P1

L1 (0.090 g, 0.210 mmol) and $Re(CO)_5Br$ (0.080 g, 0.200 mmol) were refluxed in 15 mL of toluene for 6 h. After the mixture was cooled to room temperature (RT), the solvent was removed in a water bath under reduced pressure. The resulting yellow solid was purified by silica gel column chromatography with acetic acid ethyl ester and CH_2Cl_2 (v/v = 10 : 1). Yield: 0.124 g (80%). ^{1}H NMR ($CDCl_3$, 400 MHz): δ 7.41 (3H, t, $J = 7.2$), 7.57 (3H, t, $J = 7.2$), 7.68 (3H, d, $J = 8$), 7.90 (3H, d, $J = 8$), 8.24 (3H, d, $J = 8$), 8.45 (3H, s). Anal. Calcd for $C_{34}H_{19}BrN_5O_3Re$: C, 50.31; H, 2.36; N, 8.63. Found: C, 50.65; H, 2.15; N, 8.97%. IR (KBr): v 1450, 1607, 1898, 2023, 3415 cm^{-1}.

Synthesis of P2

The procedure is similar to that of **P1**. Yield: 75%. ^{1}H NMR ($CDCl_3$, 400 MHz): δ 1.53 (18H, s), 7.52–7.55 (1H, m), 7.63 (4H, s), 7.70 (1H, m), 7.88 (2H, d, $J = 8.4$), 8.23 (2H, s), 8.39–8.48 (3H, m), 8.87 (1H, s), 9.04 (1H, s), 9.30 (1H, s), 11.41 (1H, s). Anal. Calcd for $C_{42}H_{35}BrN_5O_3Re$: C, 54.60; H, 3.82; N, 7.58. Found: C, 54.93; H, 3.45; N, 7.92%. IR (KBr): v 1454, 1608, 1905, 2026, 3417 cm^{-1}.

Synthesis of D1

The procedure is similar to that of **P1**. Yield: 78% ^{1}H NMR ($CDCl_3$, 400 MHz): δ 7.29–7.33 (5H, m), 7.39–7.47 (8H, m), 7.63–7.66 (1H, m), 7.768 (3H, m), 7.90 (3H, m), 8.09 (2H, d, $J = 6.8$), 8.15–8.21 (5H, m), 8.37 (2H, s), 8.46–8.61 (2H, m). Anal. Calcd for $C_{58}H_{33}BrN_7O_3Re$: C, 61.00; H, 2.91; N, 8.59. Found: C, 61.32; H, 2.58; N, 8.91%. IR (KBr): v 1451, 1600, 1902, 2023, 3411 cm^{-1}.

Synthesis of D2

The procedure is similar to that of **P1**. Yield: 70%. ^{1}H NMR ($CDCl_3$, 400 MHz): δ 1.46 (36H, s), 7.33 (3H, d, $J = 8.4$), 7.40–7.52 (7H, m), 7.60–7.76 (5H, m), 7.87–7.89 (1H, t, $J = 4$), 7.97 (2H, d, $J = 8$), 8.09 (1H, d, $J = 8$), 8.16–8.19 (5H, m), 8.24–8.26 (3H, m), 8.33 (1H, s), 10.19 (1H, s). Anal. Calcd for $C_{74}H_{65}BrN_7O_3Re$: C, 65.04; H, 4.79; N, 7.18. Found: C, 65.37; H, 4.43; N, 7.42%. IR (KBr): v 1476, 1602, 1908, 2024, 3423 cm^{-1}.

Spectroscopy

The IR spectra were acquired using a Magna560 FT-IR spectrophotometer. Elemental analyses were performed using a Vario Element Analyzer. ^{1}H NMR spectra were obtained using a Bruker AVANVE 400 MHz spectrometer with tetramethylsilane as the internal standard. The absorption and photoluminescence (PL) spectra of the degassed solutions with *ca.* 10^{-4} mol L^{-1} samples were recorded on a Lambda 750 spectrometer and a Hitachi model F-4500 fluorescence spectrophotometer, respectively. The LQYs were measured by comparing fluorescence intensities (integrated areas) of a standard sample (quinine sulfate) and the unknown sample according to eqn (1).

$$\Phi_{\text{unk}} = \Phi_{\text{std}}(I_{\text{unk}}/A_{\text{unk}})(A_{\text{std}}/I_{\text{std}})(\eta_{\text{unk}}/\eta_{\text{std}})^2 \qquad (1)$$

where Φ_{unk} is the LQY of the unknown sample; Φ_{std} is the LQY of quinine sulfate and taken as 0.546;[15] I_{unk} and I_{std} are the integrated fluorescence intensities of the unknown sample and quinine sulfate, respectively; A_{unk} and A_{std} are the absorbances of the unknown sample and quinine sulfate, respectively, with excitation wavelength of 365 nm. The η_{unk} and η_{std} are the refractive indices of the corresponding solvents (pure solvents were assumed). The excited-state lifetimes were detected by a system equipped with a TDS 3052 digital phosphor oscilloscope pulsed Nd:YAG laser with a THG 355 nm output and a computer-controlled digitizing oscilloscope according to the reported method.[16] The Origin 7.0 program by OriginLab Corporation was used for the curve-fitting analysis. The absorption and emission spectral data of **P1**, **P2**, **D1**, and **D2** in CH_2Cl_2 and solid state are listed in Table 1.

Crystallography

The crystals of the parent Re(I) complexes **P1** and **P2** were measured on a Bruker Smart Apex CCD single-crystal diffractometer using Mo Kα radiation, $\lambda = 0.7107$ Å at 215 K. An empirical absorption based on the symmetry-equivalent reflections was applied to the data using the SADABS program. The structure was solved using the SHELXL-97 program.[17–19]

Table 1 Photophysical parameters of **P1**, **P2**, **D1**, and **D2** in CH_2Cl_2 and solid state at 293 K

		Absorption	Excitation	Emission		
Complex	Medium	λ/nm	λ/nm	λ_{max}/nm ($W_{1/2}$/cm^{-1})	τ(A)/μs	ϕ (degassed)
P1	CH_2Cl_2	226, 262, 344, 430	256, 323, 390, 443	554 (73)		0.13
	Solid		275, 323, 478	561 (83)	0.05 (0.05), 0.29 (0.35)	
P2	CH_2Cl_2	226, 262, 284, 350,	328, 406, 452	554 (74)		0.16
	Solid		267, 333, 436, 497	553 (70)	0.05 (0.05), 0.31 (0.33)	
D1	CH_2Cl_2	238, 264, 344, 438	328, 397, 446	554 (74)		0.066
	Solid		272, 362, 458, 475	562 (89)	0.14 (0.89), 0.02 (0.03)	
D2	CH_2Cl_2	240, 268, 350, 446	322, 387, 429	554 (102)		0.0048
	Solid		274, 360, 456, 473	559 (77)	0.06 (0.07), 0.49 (0.31)	

Cyclic voltammetry

Cyclic voltammetry measurements were conducted on a voltammetric analyzer (CH Instruments, Model 620B) with a polished Pt plate as the working electrode, Pt mesh as the counter electrode, and a saturated calomel electrode (SCE) as the reference electrode, at a scan rate of 0.1 V s^{-1}. The voltammograms were recorded in CH_3CN solutions with ~10^{-3} M sample **P1**, **P2**, **D1**, and **D2** and 0.1 M tetrabutylammonium hexafluorophosphate ($TBAPF_6$) as the supporting electrolyte. Prior to each electrochemical measurement, the solution was purged with nitrogen for ~10–15 min to remove the dissolved O_2 gas.

Computational details

The geometrical structures of the ground states were optimized in gas phase by the density functional theory (DFT)[20] with Becke's LYP (B3LYP) exchange–correlation functional calculus.[21] On the basis of the optimized ground state geometry structures, the absorption spectral properties in CH_2Cl_2 media were calculated by time-dependent DFT (TDDFT),[22] associating with the polarized continuum model (PCM). The 6-31G[23, 24] basis set on C, H, N, O, and Br atoms, and LANL2DZ on Re atom were employed for all Re(I) dendrimers to ensure that the calculations were performed on the same level. The calculated electronic density plots for frontier molecular orbitals were prepared by using the GaussView 3.07 software. All the calculations were performed with the Gaussian 03 software package.[25]

Results and discussion

Synthesis and characterization

Both **R3** and **R4** were prepared from 3,6-disubstituted carbazole building blocks by copper-catalyzed Ullmann reactions. The precursors aldehydes **a**, **b**, **c**, and **d** were prepared by reactions between the carbazole derivatives of **Rn** (n = 1, 2, 3, and 4) and 4-iodobenzaldehyde, and the corresponding products were used to synthesize the dendritic ligands **L1–L4** by a condensed method.[8] Finally, the dendronized **L1–L4** were complexed to Re(I) cations to obtain the final Re(I) complexes **P1**, **P2**, **D1**, and **D2** according to the previous report,[26] and the synthetic routes to **L1–L4** and **P1**, **P2**, **D1**, and **D2** are illustrated in Scheme 1 and Scheme 2,

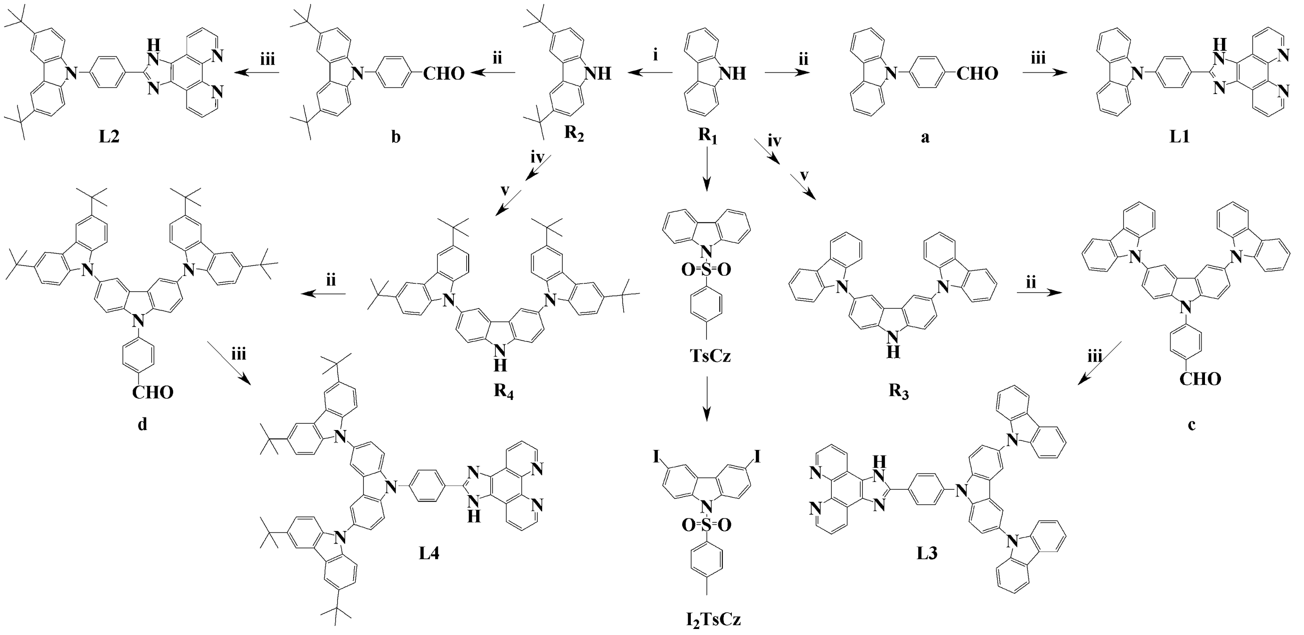

Scheme 1 Synthetic routes to **L1–L4**. (i) $AlCl_3$, ^{t}BuCl, RT, 24 h; (ii) Cu_2O, 4-iodobenzaldehyde, DMA, 170 °C, 24 h; (iii) HOAc, NH_4OAc, [1,10]phenanthroline-5,6-dione, reflux, 6 h; (iv) I_2TsCz, Cu_2O, DMAc, 170 °C, 24 h; (v) KOH, THF, DMSO, H_2O, reflux, 2 h.

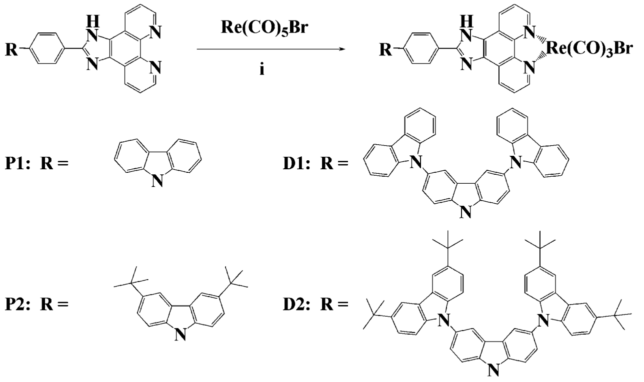

Scheme 2 Synthetic route to **P1**, **P2**, **D1**, and **D2**. (i) Toluene, N_2, reflux, 6 h.

Table 2 Crystal data for 2**P1**·$3CHCl_3$ and **P2**·CH_3OH·CH_2Cl_2

	2**P1**·$3CHCl_3$	**P2**·CH_3OH·CH_2Cl_2
Formula	$C_{71}H_{41}Br_2Cl_9N_{10}O_6Re_2$	$C_{44}H_{41}BrCl_2N_5O_4Re$
Formula weight	1981.41	1040.83
T/K	215 K	215 K
λ/Å	0.71073	0.71073
Crystal system	$P\bar{1}$	$P\bar{1}$
Space group	Triclinic	Triclinic
a/Å	11.9408(8)	11.9617(7)
b/Å	12.7779(9)	13.7719(8)
c/Å	13.1483(9)	13.8699(8)
α (°)	70.5850(10)	80.0310(10)
β (°)	88.5970(10)	66.9410(10)
γ (°)	79.0500(10)	84.7430(10)
V/Å^3	1856.0(2)	2069.9(2)
Z	1	2
ρ_c/Mg m^{-3}	1.773	1.670
μ/mm^{-1}	4.716	4.079
F(000) (e)	958	1032
Range of transm factors (deg)	2.44–25.95	1.61–28.31
Reflns collected/ unique	9935/6956	13152/9549
R(int)	0.0257	0.0333
Completeness	97.1% (θ = 25.00)	99.4% (θ = 25.00)
R_1, wR_2 [$I > 2\sigma(I)$]	0.0789/0.2220	0.0482/0.1022
R_1, wR_2 (all data)	0.0940/0.2366	0.0769/0.1141

respectively. The structures of the four synthesized Re(I) complexes were fully verified with IR, UV–Vis, elemental analysis, and ^{1}H NMR spectroscopy.

The needle-like yellow crystals for **P1** and **P2** were obtained at RT over a period of a week from the evaporation of the solutions of **P1**–methanol–chloroform and **P2**–methanol–dichloromethane, respectively. The solid-state structures of **P1** and **P2** were determined by single-crystal X-ray diffraction and the ORTEP diagrams of **P1** and **P2** are presented in Fig. 1. The crystal data of **P1** and **P2** are listed in Table 2, while the selected bond distances and the angles are listed in Table S1†. The coordination geometry at the Re cations is a distorted octahedron with the three carbonyl ligands arranged in a facial fashion, and the coordination atmospheres of the Re atoms in **P1** and **P2** are similar to each other. For example, the bond distance of Br–Re and the average bond distances of Re–C and Re–N are 2.6246(7), 1.915, and 2.1785 Å for **P1**, and 2.617(4), 1.883, and 2.105 Å for **P2**, respectively. The bond angles in Table S1† clearly indicate that the CO ligands are almost linearly coordinated. The bond angles between the adjacent CO carbon atoms in **P1** and **P2** are within the ranges 87.5(3)–89.8(3)° and 88.4(3)–90.4(3)°, respectively, which are close to 90°. But the N–Re–N angles in **P1** (75.64(17) °) and **P2** (75.75 (19) °) are much smaller than 90°, which is most likely due to the result of the steric requirement of the bidentate coordination of **L1** and **L2**. At the same time, the planes of the pyrrole ring and the imidazole ring of **P1** and **P2** which are connected by a phenylene intersect at angles of 7.38° and 18.42°, respectively. The serious thermal vibration of the solvent molecules in the single crystal structure of **P1** leads to

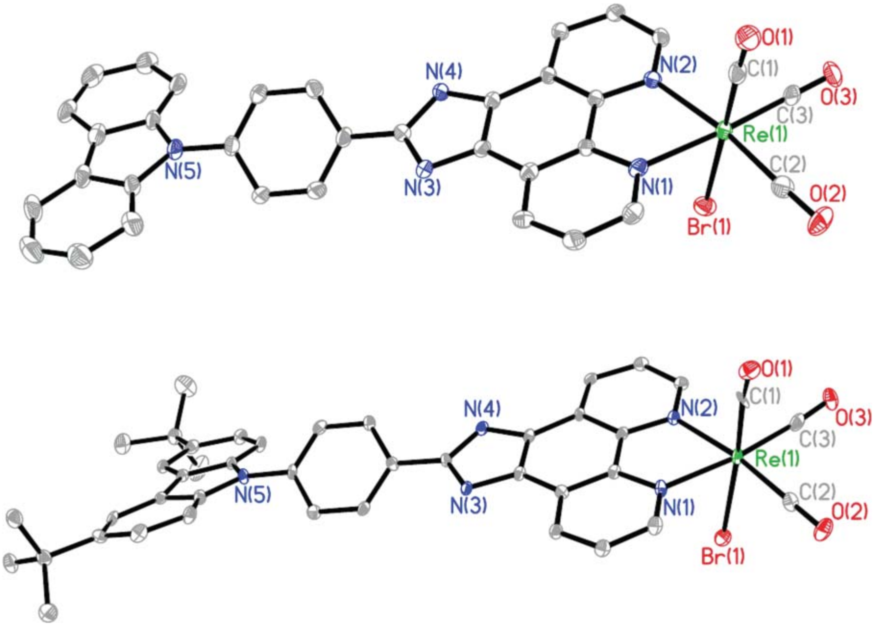

Fig. 1 ORTEP drawing of the crystal of **P1** (upper) and **P2** (lower) with displacement ellipsoids at the 30% probability level. Hydrogen atoms are omitted for clarity.

the disorder of C(35) and Cl(1)–Cl(3) and the bigger temperature factors of C(36) and Cl(4)–Cl(6).

Electrochemistry

Cyclic voltammograms of **P1**, **P2**, **D1**, and **D2** presented in Fig. 2 exhibit irreversible redox behaviors in CH_3CN solution. The anodic waves of these Re(I) dendrimers are associated with a Re^{I}-based oxidation process (Re^{I}/Re^{II}), and the cathodic waves are associated with a ligand-based reduction process ($[Re^{I}Br(CO)_3(L)]/[Re^{I}Br(CO)_3(L^{\bullet})]^{-}$).[27] As presented in Fig. 2, **P1** shows an anodic wave peak at +1.41 V with the onset oxidation potential (V_{onset}) of +1.08 V and cathodic wave peak at –1.44 V with the V_{onset} of –1.34 V. For **P2**, the anodic wave and cathodic wave peaks shift to + 1.22 V with V_{onset} of +1.09 V and –1.40 V with the V_{onset} of –1.29 V, respectively. For **D1** and **D2**, the peaks of the anodic waves are located at + 1.27 V with the V_{onset} of +1.11 V and + 1.21 V with the V_{onset} of +1.13 V, and the peaks of the cathodic waves are located at –1.46 V with the V_{onset} of –1.33 V and –1.39 V with the V_{onset} of –1.29 V, respectively. The energy levels of the highest-occupied molecular orbital (HOMO) and the lowest-unoccupied molecular orbital (LUMO) are calculated from the onset potentials of the oxidation (E_{onset}(Ox)) and reduction (E_{onset}(Red)) peaks with the formula $E_{HOMO} = -4.74 - E_{onset}(Ox)$ and $E_{LUMO} = -4.74 - E_{onset}(Red)$ (–4.74 V for SCE with respect to the zero vacuum level,[28]) respectively. These calculations give the E_{HOMO}s of –5.82, –5.83, –5.85 and –5.87 eV, and the E_{LUMO}s of –3.40, –3.45, –3.41, and –3.45 eV for **P1**, **P2**, **D1**, and **D2**, respectively. As presented above, both the carbazole (Cz) group and the *tert*-butyl group in the Re(I) complexes lower the molecular orbital energy levels in CH_3CN solution. As a result, the order of the E_{HOMO} is: **P1** > **P2** > **D1** > **D2**, and the order of the E_{LUMO} is **P1** > **D1** > **P2** = **D2**.

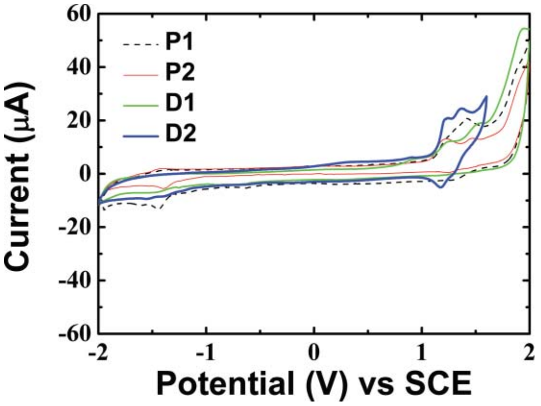

Fig. 2 Cyclic voltammograms of **P1**, **P2**, **D1**, and **D2** measured in CH_3CN (vs SCE) at a scan rate of 0.1 V s^{-1}. A polished Pt plate and a Pt mesh were used as the working electrode and the counter electrode, respectively. $TBAPF_6$ was taken as supporting electrolyte.

Photophysical properties

Fig. 3 shows UV–Vis absorption and the excitation spectra of **P1**, **P2**, **D1**, and **D2** in CH_2Cl_2. The dominant absorption bands of **P1**, **P2**, **D1**, and **D2** in the *ca.* 220–400 nm region should be assigned to the ligand-centred $\pi \rightarrow \pi^*$ absorptions. These bands are also accompanied by the lower-energy features extending into the visible region from *ca.* 400 to *ca.* 500 nm, which are tentatively assigned to the MLCT transitions. These assignments are based on the absorption spectra of the free ligands[5] shown in Fig. S1 (ESI†) and the theoretical studies (vide infra).

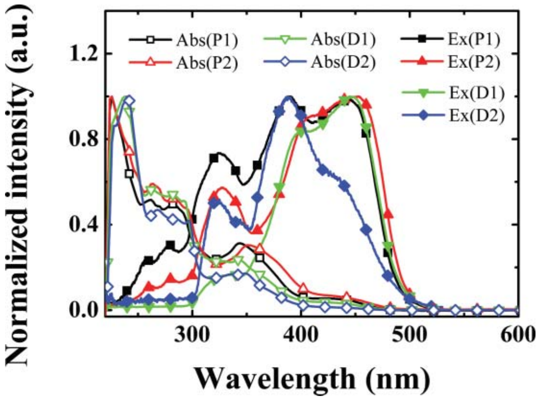

Fig. 3 Absorption and excitation spectra of **P1**, **P2**, **D1**, and **D2** in CH_2Cl_2.

Fig. 4 shows the PL spectra of **P1**, **P2**, **D1**, and **D2** in CH_2Cl_2. The PL spectra of these samples, except that the width of the half maximum ($W_{1/2}$) of **D2** is *ca.* 102 nm (Table 1), present similar emission bands peaking at *ca.* 554 nm with $W_{1/2}$ of *ca.* 74 nm. The LQYs of **P1**, **P2**, and **D1** are measured to be 0.13, 0.16, and 0.066, respectively, which are much higher than that of the reported **Re3** (0.03).[12] But the LQY of **D2** (0.0048) is almost six times lower than that of **Re3**, which should be partly attributed to the more pliable molecular structures of **D2** in CH_2Cl_2 with the addition of the *tert*-butyl groups.[12] The broad and low-energy band in the absorption spectra partially resolve into two bands in scanning the excitation spectra, namely, ^{1}MLCT transition states with peaks at 390, 410, 401, and 388 nm and ^{3}MLCT transition states with peaks at 444, 453, 445, and 434 nm for **P1**, **P2**, **D1**, and **D2**, respectively.[26,29] Excitation at either the $\pi \rightarrow \pi^*$ absorption region (~ 324 nm) or the MLCT absorption region (~ 386 nm for **P1** and **D2**, ~ 450 nm for **P2** and **D1**) leads to the same MLCT emission band at RT for **P1**, **P2**, **D1**, and **D2**, which indicates there should be a potential surface crossing (PSC) from the higher $\pi \rightarrow \pi^*$ state to the lower MLCT state, and the major contribution of the observed emission is from the latter.[30] This character of the PL spectra is further revealed by the measurement of the excited-state lifetimes.

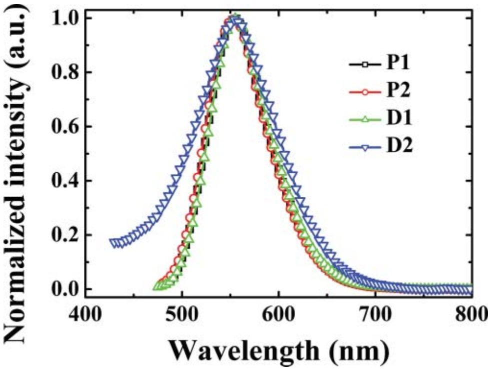

Fig. 4 PL spectra of **P1**, **P2**, **D1**, and **D2** in CH_2Cl_2.

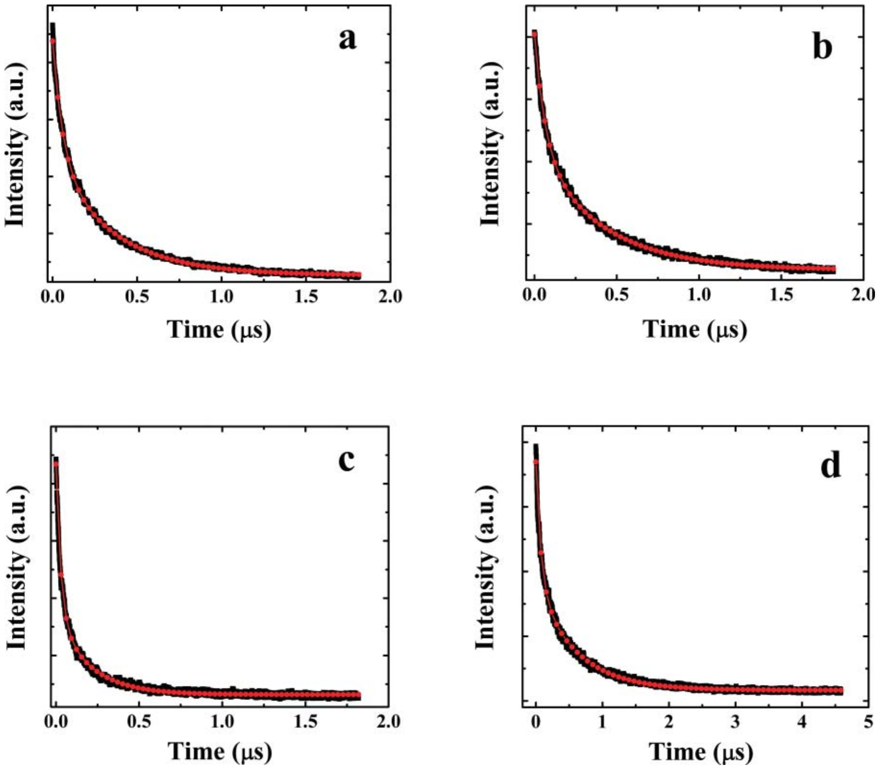

Fig. 5 PL lifetime decay measurements of the powder samples of **P1** (a), **P2** (b), **D1** (c), and **D2** (d).

As indicated in Fig. 5, the PL spectra are composed of biexponential decays with $\tau_1 = 0.05$ (A_1=0.053), 0.05 (A_1=0.05), 0.14 (A_1=0.89), 0.06 μs (A_1=0.07), and $\tau_2 = 0.29$ (A_2=0.35), 0.31 (A_2=0.33), 0.02 (A_2=0.03), 0.49 μs (A_2=0.31) for **P1**, **P2**, **D1**, and **D2**, respectively. In general, if there is PSC from the higher $\pi \rightarrow \pi^*$ state to the lower MLCT state, then strong excitation bands in the $\pi \rightarrow \pi^*$ absorption region and a shorter decay lifetime from the $\pi \rightarrow \pi^*$ state than those from the lower MLCT state should be observed based on the energy law.[31] As can be seen from Fig. 3, the strength of the excitation peaks of the samples show the following order: **P1** > **P2** > **D2** >> **D1** in the $\pi \rightarrow \pi^*$ absorption region with the normalization according to the maximum peak values, suggesting that the order of the efficiency of the PSC from the $\pi \rightarrow \pi^*$ state to the MLCT state should be in the same order. Therefore, the assignment of τ_1 of **P1**, **P2**, **D1**, and **D2** to the emission from the $\pi \rightarrow \pi^*$ state should be reasonable.[29] The average lifetimes ($\bar{\tau}$) of **P1**, **P2**, **D1**, and **D2** are calculated according to eqn (2).

$$\bar{\tau} = (A_1\tau_1 + A_2\tau_2)/(A_1 + A_2) \tag{2}$$

The average lifetimes of **P2** (0.28 μs) and **D2** (0.41 μs) are longer than those of **P1** (0.26 μs) and **D1** (0.14 μs), respectively, suggesting that the attachment of the *tert*-butyl substituents to **P2** and **D2** is helpful in extending their radiative lifetimes due to the fact that the bigger molecular radii will reduce the T–T annihilation between the light-emitting centers.

Theoretical calculations

Frontier molecular orbital properties. As can be seen from Table S1,† the selected bond distances and the angles of the simulated molecular structures of **P1** and **P2** are nicely coincident with those from the experimental measurements: the bond distance of Br–Re and the average bond distances of Re–C and Re–N of **P1**, which are the same as those of **P2**, are calculated to be 2.677, 1.921 and 2.186 Å, respectively. The difference between these parameters and those from the experimental measurements is less than 0.06 Å. The calculated bond angles of C–Re–C and O–C–Re are within the ranges 90.7–92.2° and 177.2–179.8° for **P1** and **P2**, respectively, indicating that the CO ligands almost linearly coordinate to Re ions, and have an angle of close to 90° between them. The difference between the theoretical calculations and the experimental measurements should be attributed to the fact that the former are optimized in the gas phase and the latter are in a tight crystal lattice.[32]

As can be seen from Fig. S2–S5,† the LUMOs of **P1**, **P2**, **D1**, and **D2**, which have similar distribution, are composed of the π^* orbitals localized on the 1*H*-imidazo[4,5-f][1,10]phenanthroline (**L′**) moiety with *ca.* 90% composition (Table S2 and S3†), while their LUMO+1 and LUMO+2 extend to the π^* orbitals of the bridging phenylene. The LUMO+3 of **P1** (**P2**) is mainly composed of the π^* orbitals localized on almost the whole **L** ligand, while that of **D1** (**D2**) is mainly composed of the π^* orbitals localized on **R3** (**R4**).

The HOMO and HOMO−1 of **P1** (**P2**) are mainly composed of the π orbitals of the carbonyl group, the bromine, and the d orbitals of Re cations which are in antibonding coordination with the axial bromine group and bonding with the three carbonyl groups, while those of **D1** (**D2**) are localized predominantly on the π-conjugated [9,3′;6′,9″]tercarbazole (TCz) moiety. The HOMO−2 and the HOMO−3 of **P1** (**P2**) are mainly composed of the π orbitals of the carbazole moiety, and the composition of the HOMO−2 and the HOMO−3 of **D1** (**D2**) are similar to

Table 3 Selected singlet-absorption parameters of **P1**, **P2**, **D1**, and **D2** in CH_2Cl_2 according to TDDFT (LANL2DZ/6-31G) calculations

Complex	State	Transition	λ/nm/E/eV	Oscillator	Assignment	λ_{exp}/nm
P1	S_1	H–1 → L (97%)	482/2.57	0.0036	d→π*/π→π*	430
	S_4	H → L+1 (100%)	421/2.95	0.2561	d→π*/π→π*	
	S_{10}	H → L+2 (98%)	370/3.35	0.3959	d→π*/π→π*	344
	S_{14}	H–4 → L+1 (73%)	334/3.72	0.0907	d→π*/π→π*	
	S_{22}	H → L+5 (93%)	304/4.07	0.1041	d→π*/π→π*	282
	S_{26}	H–4 → L+2 (78%)	296/4.19	0.3087	d→π*/π→π*	
P2	S_1	H → L (100%)	501/2.47	0.0535	d→π*/π→π*	450
	S_4	H → L+1 (100%)	439/2.82	0.2310	d→π*/π→π*	
	S_{13}	H–4 → L+1 (84%)	336/3.69	0.1374	d→π*/π→π*	350
	S_{29}	H–4 → L+2 (79%)	296/4.19	0.4086	d→π*/π→π*	
	S_{32}	H–9 → L (48%)	287/4.31	0.1494	d→π*/π→π*	284
	S_{37}	H–9 → L+1 (55%)	274/4.53	0.4259	d→π*/π→π*	
D1	S_1	H → L (100%)	510/2.43	0.0189	π→π*	438
	S_9	H–3 → L (46%)	406/3.06	0.0214	d→π*/π→π*	
	S_{12}	H → L+2 (100%)	391/3.17	0.2590	π→π*	
	S_{24}	H–5 → L+2 (76%)	336/3.69	0.1291	π→π*	342
	S_{31}	H–8 → L+1 (55%)	322/3.86	0.3513	π→π*	
	S_{54}	H–15 → L (29%)	286/4.34	0.1333	π→π*	282
D2	S_1	H → L (100%)	534/2.32	0.0133	π→π*	446
	S_8	H–3 → L (100%)	421/2.94	0.0003	d→π*/π→π*	
	S_{10}	H → L+2 (100%)	402/3.08	0.2333	π→π*	
	S_{22}	H-4 → L+2 (79%)	335/3.70	0.4231	π→π*	336
	S_{31}	H–11 → L+1 (31%)	322/3.85	0.1946	π→π*	
	S_{52}	H–8→ L+2 (74%)	292/4.24	0.2512	π→π*	298

the HOMO and the HOMO–1 of **P1** (**P2**), respectively. These results present that the difference among the diimine ligands **L1–L4** dramatically influences the distribution of the occupied molecular orbitals in the corresponding Re(I) dendrimers, which should also result in the different electronic transition character upon excitation.

As presented in Table S2 and Table S3, the theoretical calculations on the E_{HOMO} of **P1**, **P2**, **D1**, and **D2** exhibit the order **P1** (–5.51 eV) < **P2** (–5.49 eV) < **D1** (–5.42 eV) < **D2** (–5.23 eV), while their E_{LUMO}s exhibit the order **P2** (–2.76 eV) > **P1** (–2.78 eV) > **D2** (–2.85 eV) > **D1** (–2.87). The different orders of the E_{HOMO}s and E_{LUMO}s of **P1**, **P2**, **D1**, and **D2** between the experimental measurements and the theoretical calculations should be attributed to the fact that the solution effect is ignored during the optimization of the geometrical structures of their ground states.

Absorption spectra. The curves of the theoretically simulated absorption spectra of **P1**, **P2**, **D1**, and **D2** presented in Fig. 6 are nicely fitted to those from the experimental measurements. As presented in Table 3, the lowest lying singlet → singlet absorptions of **P1**, **P2**, **D1**, and **D2** are calculated at 482, 501, 510, and 534 nm, respectively. The absorption of **D1** (**D2**) is red-shifted according to that of **P1** (**P2**), which should be attributed to the intense participation of the TCz part which narrows the energy gaps between the HOMOs and LUMOs of **D1** and **D2**[32] (Fig. 7). The configuration of HOMO–1 → LUMO is responsible for the lowest lying transition of **P1**, while that of HOMO → LUMO is responsible for those of **P1**, **P2**, **D1**, and **D2**. The HOMO–1 of **P1** is mainly composed of *ca.* 17.5% Re(I) d orbital (13.9% d_{xz} +3.6% d_{xy}), 11.1% carbonyl group, and 59.6% bromine group. The LUMO of **P1**, which is similar to those of **P2**, **D1**, and **D2**, is a π^* (90.4%, L′) type orbital in nature. Thus, the transition at 482 nm for **P1** should be described as the metal/ligand-to-

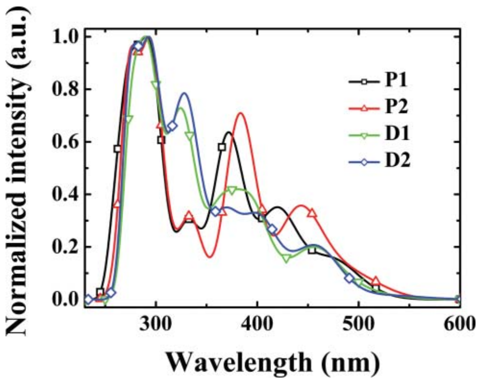

Fig. 6 Simulated absorption spectra of **P1**, **P2**, **D1**, and **D2** at the TDDFT (B3LYP)/6-31G level in CH_2Cl_2.

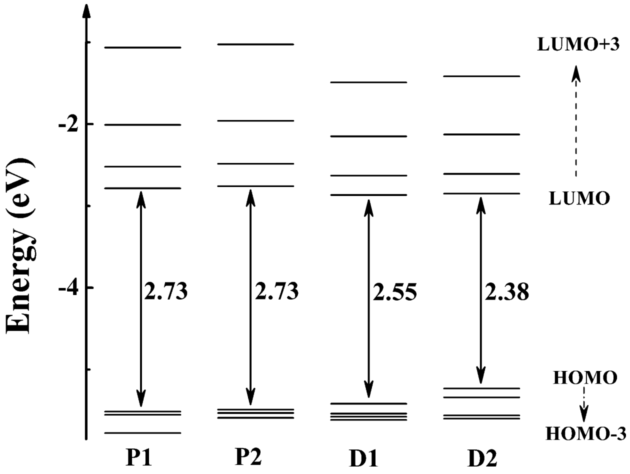

Fig. 7 Pictorial representation of the frontier molecular orbital energy levels of **P1**, **P2**, **D1**, and **D2** calculated in the gas phase at the DFT/B3LYP/6-31G level.

ligand charge transfer [d(Re) + π(CO+Br)] → [π*(L)] (MLLCT) transition. The composition of the HOMO of **P2** is similar to that of the HOMO−1 of **P1** in nature, as a result, the lowest lying transition at 501 nm for **P2** is similar to that of **P1**. The HOMOs of **D1** and **D2** are mainly composed of *ca.* 97.2% **R3** and 97.7% **R4**, respectively, and the transitions of **D1** at 510 nm and **D2** at 534 nm should be attributed to the π (**R3** for **D1** and **R4** for **D2**) → π*(L′)transitions. The absorptions with the largest oscillator strength at 370, 296, 322, and 335 nm are in agreement with the experimental values of 344, 284, 342, and 350 nm for **P1**, **P2**, **D1**, and **D2**, respectively. The dominant character of these higher energy absorptions is the MLLCT and π → π* transitions for **P1** (**P2**) and **D1** (**D2**), respectively. The excitation of HOMO → LUMO+2 (98%) contributes to the absorption at 370 nm of **P1**. The HOMO of **P1** is mainly composed of *ca.* 20% metal Re(I) d orbital (11.4 d_{z^2} + 5.1d_{yz} + 3.4$d_{x^2-y^2}$), 14.4% carbonyl group, and 57.2% bromine group, while its LUMO+2 is π*(L′) orbital in nature, thus the absorption is tentatively attributed to the MLLCT transitions. The excitations of HOMO−8 → LUMO+2 for **D1** and HOMO−4 → LUMO+2 for **D2**, which contribute 55% and 79% of the absorptions at 322 and 335 nm, respectively, should be mainly attributed to π → π* absorptions (Table 3). According to the fact that the HOMO−4 of **P2** is composed of *ca.* 66% Re d orbital which is much larger than those of the HOMO of **P1** (20%), the HOMO−8 of **D1** (none), and the HOMO−4 of **D2** (none), the MLCT component contribution to the transition with the largest oscillator strength in **P2** should be much larger than those of **P1**, **D1**, and **D2**. At the same time, the absorptions with moderate oscillator strength are calculated to be the MLLCT and the π → π* absorptions for **P1** (**P2**) and **D1** (**D2**), respectively.

The configurations of HOMO → LUMO of **P1**, **P2**, **D1**, and **D2** are responsible for the corresponding lowest lying triplet → triplet absorptions at 507, 521, 517, and 543 nm for **P1**, **P2**, **D1**, and **D2**, respectively (Table S4†). Therefore these transitions are similar to the corresponding lowest lying singlet → singlet absorptions of **P1**, **P2**, **D1**, and **D2**, respectively. De Angelis *et al.*[33] and Chou *et al.*[34,35] found that the intersystem crossing could be enhanced by the notable MLCT transition participation, namely, the phosphorescence ($T_1 \rightarrow S_0$ radiative transition) in which the π → π* transitions mixed with MLCT transitions should be greatly increased by increasing the ratio between MLCT transitions and the π → π* transitions. Additionally, Abrahamsson *et al.* also concluded that the LQY could be partly increased by the larger proportion of MLCT transitions.[36] Our deduction that the greater contribution of MLCT transitions in **P1** and **P2** than in **D1** and **D2** can be partly attributed to the fact that the LQYs of **P1** (0.13) and **P2** (0.16) are higher than those of **D1** (0.066) and **D2** (0.0048) in CH_2Cl_2 is consistent with these conclusions, which suggests that the purposely designed dendron ligands should be helpful to improve the PL properties of Re(I) complexes.

Conclusions

Re(I) complexes **P1**, **P2**, **D1**, and **D2** with similar PL spectra peaked at 554 nm are synthesized, and their photophysical behavior is experimentally and theoretically studied. **P1**, **P2**, **D1**, and **D2** display biexponential light-emitting properties with average lifetimes of 0.26, 0.28, 0.14, and 0.41 μs, respectively, which indicates that the *tert*-butyl groups in **P2** and **D2** are helpful in extending their radiative lifetimes. The LQYs of **P1** and **P2** are measured to be 0.13 and 0.16 which are much higher than those of **D1** (0.066), **D2** (0.0048), and the previously reported **Re3** (0.03).

Acknowledgements

The authors are grateful for financial aid from the National Natural Science Foundation of China (Grant No. 20631040 and 20771099) and the MOST of China (Grant No. 2006CB601103, 2006DFA42610).

References

1 E. Fujita, B. S. Brunschwig, T. Ogata and S. Yanagida, *Coord. Chem. Rev.*, 1994, **132**, 195.
2 N. Sutin, C. Creutz Fujita and E. Comments, *Comments Inorg. Chem.*, 1997, **19**, 67.
3 F. P. A. Johnson, M. W. George, F. Hartle and J. J. Turner, *Organometallics*, 1996, **15**, 3374.
4 W. Zhan, J. Alvarez and R. M. Crooks, *J. Am. Chem. Soc.*, 2002, **124**, 13265.
5 Y.-M. Cheng, G.-H. Lee, P.-T. Chou, L.-S. Chen, Y. Chi, C.-H. Yang, Y.-H. Song, S.-Y. Chang, P.-I. Shih and C.-F. Shu, *Adv. Funct. Mater.*, 2008, **18**, 183.
6 V. Balzani and A. Juris, *Coord. Chem. Rev.*, 2001, **211**, 97.
7 S. Welter, K. Brunner, J. W. Hofstraat and L. De Cola, *Nature*, 2003, **421**, 54.
8 C. Liu, J. Li, B. Li, Z. Hong, F. Zhao, S. Liu and W. Li, *Appl. Phys. Lett.*, 2006, **89**, 243511.
9 L.-O. Pålsson, R. Beavington, M. J. Frampton, J. M. Lupton, S. W. Magennis, J. P. J. Markham, J. N. G. Pillow, P. L. Burn and I. D. W. Samuel, *Macromolecules*, 2002, **35**, 7891.
10 M. Guan, Z. Q. Bian, F. Y. Li, H. Xin and C. H. Huang, *New J. Chem.*, 2003, **27**, 1731.
11 J.-L. Wang, J. Yan, Z.-M. Tang, Q. Xiao, Y. Ma and J. Pei, *J. Am. Chem. Soc.*, 2008, **130**, 9952.
12 Y.-J. Pu, R. E. Harding, S. G. Stevenson, E. B. Namdas, C. Tedeschi, J. P. J. Markham, R. J. Rummings, P. L. Burn and I. D. W. Samuel, *J. Mater. Chem.*, 2007, **17**, 4255.
13 G. Accorsi, A. Listorti, K. Yoosaf and N. Armaroli, *Chem. Soc. Rev.*, 2009, **38**, 1690.
14 T. Xu, R. Lu, X. Liu, P. Chen, X. Qiu and Y. Zhao, *Eur. J. Org. Chem.*, 2008, 1065.
15 K. Ye, J. Wang, H. Sun, Y. Liu, Z. Mu, F. Li, S. Jiang, J. Zhang, H. Zhang, Y. Wang and C.-M. Che, *J. Phys. Chem. B*, 2005, **109**, 8008.
16 J. M. Villegas, S. R. Stoyanov and D. P. Rillema, *Inorg. Chem.*, 2002, **41**, 6688.
17 G. M. Sheldrick, *SHELXTL, version 5.10*, Siemens Analytical X-ray Instruments Inc.: Madison, WI, 1998.
18 *SMART and SAINT*, Siemens Analytical X-ray Instruments Inc.: Madison, WI, 1995.
19 G. M. Sheldrick, *SADABS*, University of Göttingen: Göttingen, Germany, 1996.
20 E. Runge and E. K. U. Gross, *Phys. Rev. Lett.*, 1984, **52**, 997.
21 S. L. Mayo, B. D. Olafso and W. A. Goddard, *J. Phys. Chem.*, 1990, **94**, 8897.
22 J. Autschbach, T. Ziegler, S. J. A. Gisbergen and E. J. Baerends, *J. Chem. Phys.*, 2002, **116**, 6930.
23 D. M. Dattelbaum, K. M. Omberg, P. J. Hay, N. L. Gebhart, R. L. Martin, J. R. Schoonover and T. J. Meyer, *J. Phys. Chem. A*, 2004, **108**, 3527.
24 N. J. Lundin, P. J. Walsh, S. L. Howell, J. J. McGarvey, A. G. Blackman and K. C. Gordon, *Inorg. Chem.*, 2005, **44**, 3551.
25 M. J. Frisch, G. W. Trucks, H. B. Schlegel, G. E. Scuseria, M. A. Robb, J. R. Cheeseman, J. A. Montgomery, Jr., T. Vreven, K. N. Kudin, J. C. Burant, J. M. Millam, S. S. Iyengar, J. Tomasi, V. Barone, B. Mennucci, M. Cossi, G. Scalmani, N. Rega, G. A. Petersson, H. Nakatsuji, M. Hada, M. Ehara, K. Toyota, R. Fukuda, J. Hasegawa, M. Ishida, T. Nakajima, Y. Honda, O. Kitao, H. Nakai, M. Klene, X. Li, J. E. Knox, H. P. Hratchian, J. B. Cross, V. Bakken, C. Adamo, J. Jaramillo, R. Gomperts, R. E. Stratmann, O. Yazyev, A. J. Austin, R. Cammi,

C. Pomelli, J. Ochterski, P. Y. Ayala, K. Morokuma, G. A. Voth, P. Salvador, J. J. Dannenberg, V. G. Zakrzewski, S. Dapprich, A. D. Daniels, M. C. Strain, O. Farkas, D. K. Malick, A. D. Rabuck, K. Raghavachari, J. B. Foresman, J. V. Ortiz, Q. Cui, A. G. Baboul, S. Clifford, J. Cioslowski, B. B. Stefanov, G. Liu, A. Liashenko, P. Piskorz, I. Komaromi, R. L. Martin, D. J. Fox, T. Keith, M. A. Al-Laham, C. Y. Peng, A. Nanayakkara, M. Challacombe, P. M. W. Gill, B. G. Johnson, W. Chen, M. W. Wong, C. Gonzalez and J. A. Pople, *GAUSSIAN 03*, Gaussian, Inc., Wallingford, CT, 2004.

26 Z. Si, J. Li, B. Li, F. Zhao, S. Liu and W. Li, *Inorg. Chem.*, 2007, **46**, 6155.

27 S. Berger, A. Klein, W. Kaim and J. Fiedler, *Inorg. Chem.*, 1998, **37**, 5664.

28 J. Bard and L. R. Faulkner, *Electrochemical Methods Fundamental and Applications*, Wiley: New York, 1980.

29 S. Ranjan, S.-Y. Lin, K. C. Hwang, Y. Chi, W.-L. Ching, C.-S. Liu, Y.-T. Tao, C.-H. Chien, S.-M. Peng and G.-H. Lee, *Inorg. Chem.*, 2003, **42**, 1248.

30 L. Sacksteder, A. P. Zipp, E. A. Brown, J. Streich, J. N. Demas and B. A. DeGraff, *Inorg. Chem.*, 1990, **29**, 4335.

31 L. Wallace and D. P. Rillema, *Inorg. Chem.*, 1993, **32**, 3836.

32 X. Li, X. Liu, Z. Wu and H. Zhang, *J. Phys. Chem. A*, 2008, **112**, 11190.

33 F. De Angelis, S. Fantacci, N. Evans, C. Klein, S. M. Zakeeruddin, J.-E. Moser, K. Kalyanasundaram, H. J. Bolink, M. Grätzel and M. K. Nazeeruddin, *Inorg. Chem.*, 2007, **46**, 5989.

34 P. T. Chou and Y. Chi, *Chem.–Eur. J.*, 2007, **13**, 380.

35 Y. Chi and P. T. Chou, *Chem. Soc. Rev.*, 2007, **36**, 1421.

36 M. Abrahamsson, L. Hammarström, D. A. Tochere, S. Nag and D. Datta, *Inorg. Chem.*, 2006, **45**, 9580.